中国科学: 物理学 力学 天文学 2023 年 第 53 卷 第 4 期: 244612
SCIENTIA SINICA Physica, Mechanica & Astronomica physcn.scichina.com
《中国科学》杂志社 SCIENCE CHINA PRESS
论 文

韧性材料在球形压头渐进载荷下仪器化划入行为

刘明*, 徐智通

福州大学机械工程及自动化学院, 福建省太赫兹功能器件与智能传感重点实验室, 福州 350108
*联系人, E-mail: mingliu@fzu.edu.cn

收稿日期: 2022-10-24; 接受日期: 2023-01-16; 网络出版日期: 2023-03-21
国家自然科学基金(编号: 51705082)、福建省闽江学者特聘教授(编号: 0020-510759)、福州大学旗山学者海外人才引进计划(编号: 0020-650289)和晋江市福大科教园区发展中心科研项目(编号: 2019-JJFDKY-11)资助

摘要 使用半径为500 μm的球形氧化锆陶瓷压头对3种高分子和20种金属材料在渐进载荷下进行微米划入测试, 研究了韧性材料在球形压头仪器化划入过程中的弹塑性变形行为. 仪器化划入结果发现: 随载荷的增加, 金属的弹性回复率、残余划痕硬度、几何划痕硬度和侧向划痕硬度均趋于稳定. 而高分子的弹性回复率, 几何划痕硬度却是单调减小, 很有可能产生损伤破坏, 在最大载荷下利用线弹性断裂力学方法计算得到的断裂韧度与文献中的结果一致; 在大载荷下, 残余划痕硬度和侧向划痕硬度趋近于常数. 残余划痕硬度大于几何划痕硬度; 摩擦系数随着载荷的增大而非线性增大是由于球形压头几何形状的影响(灰口和球墨铸铁的摩擦系数平稳段是由于石墨的影响). 大部分材料的划入响应与力学性能有密切关系: 临界划痕应变(弹性回复率平稳阶段的起始应变)与屈服应变成正比; 趋于稳定的残余划痕硬度与屈服强度有线性关系, 并且与努氏硬度成比例.

关键词 仪器化划入, 球形压头, 渐进载荷, 弹塑性变形, 力学性能

PACS: 46.35.+z, 46.55.+d, 46.80.+j, 61.41.+e, 62.20.Fe

1 引言

仪器化划入是一种表征材料表面微观力学性能和摩擦学性能的试验手段[1], 广泛应用于研究各种材料(玻璃[2,3]、高分子[4,5]、复合材料[6,7])的摩擦学行为[8–11]、抗划擦能力[12,13]、划痕诱导的破坏/裂纹[14,15]、摩擦系数[16–23]、涂层的结构完整性[14,15]、膜基结合力[24]、划痕硬度[25,26]、断裂韧度[10,11,27–32]等. 划入测试时, 将一个硬质压头法向压入材料, 同时以一定的速度沿材料表面切向运动, 压头前方和后方的材料分别承受压应力和拉应力[33], 应力场很复杂, 材料堆积较严重[34]. 仪器化划入是仪器化压入的新形式, 仪器化压入中只有法向载荷, 没有侧向加载[35,36]; 而仪器化划入多了侧向的位移和载荷. 仪器化划入和压入有很多相似之处(比如塑性变形相似)[37,38], 研究压入的理论和方法也可以应用于仪器化划入, 都可以获得压入深度和法向力, 法向方向的力和位移的加载曲线在小载荷下非常相似, 但大载荷下相差较大, 这是因为侧向力(或切向力)会导致更大的塑性变形和压入深度[16]. 仪器化划入也可以定义划入硬

引用格式: 刘明, 徐智通. 韧性材料在球形压头渐进载荷下仪器化划入行为. 中国科学: 物理学 力学 天文学, 2023, 53: 244612
Liu M, Xu Z T. Scratch responses of ductile materials by instrumented scratch with a spherical indenter under progressive load (in Chinese). Sci Sin-Phys Mech Astron, 2023, 53: 244612, doi: 10.1360/SSPMA-2022-0402

© 2023 《中国科学》杂志社

度有一定的关系[39,40].

材料的弹塑性参数与仪器化划入响应之间有一定内在联系. Zhang等人[41]利用深度学习确定了金属材料的仪器化划入响应与塑性力学参数(如屈服应力和应变硬化指数)之间的关系. Zhang等人[42]结合量纲和有限元分析, 提出了通过仪器化划入获取金属材料塑性力学参数和界面摩擦系数的方法. Ovaert等人[43]利用纳米压痕, 仪器化微米划入和有限元方法评估了高分子涂层的抗拉强度. Bellemare等人[44]利用仪器化摩擦滑动试验获取了金属材料的屈服强度和应变硬化指数等塑性性能. Belov等人[45]利用仪器化划入实验方法测得了有机涂层的界面结合力和强度参数. Huang等人[46]利用纳米划入评估了类金刚石薄膜的弹塑性力学性能和断裂机理. Xiang等人[47]研究了高分子材料的弹塑性力学性能与仪器化划入响应之间的关系. Bellemare等人[48]结合有限元和量纲分析量化了金属材料塑性变形特征对摩擦滑动响应的影响. Beake等人[49]研究了弹塑性力学性能对TiN/Si_3N_4涂层的纳米划入响应的影响. Hara等人[50]研究了涂层的粘弹性能与划痕形貌的关系. Burnett等人[51]探讨了涂层硬度与界面结合力之间的关系. 仪器化压入和划入方法均可表征脆性材料(微波介电陶瓷[28]和半导体材料(单晶硅和碳化硅)[32])的断裂韧度. 断裂韧度综合体现材料的强度和韧性, 反映了材料抵抗裂纹失稳扩展的能力. 仪器化划入表征材料断裂韧度的前提条件需要压头前方产生裂纹[37,52], 但不同材料在何种加载条件下才会产生满足条件的裂纹还需进一步探究[28].

张亚锋等人[53]使用原子力显微镜对不同类型的玻璃进行仪器化纳米划入试验, 发现材料表层的机械性能会影响划痕的残余深度. Pöhl等人[54]对纯铁进行仪器化划入试验, 发现纯铁的低强度和较低加工硬化能力会产生较大的划痕深度, 并在划痕两侧产生大量的材料堆积. 谢祖飞等人[55]研究了载荷对材料摩擦机制的影响, 发现材料的硬度和弹性模量对摩擦机制有显著影响, 当硬度越高时, 材料不容易发生犁沟损伤. 压头形状对材料的仪器化划入行为有重要影响, 为研究材料在圆球压头划入过程的弹塑性变形行为, 对常见工程韧性材料在球形压头渐进载荷下进行了仪器化划入测试, 揭示了摩擦系数、压入深度、残余深度、弹性恢复率、划痕宽度、划痕硬度等随载荷的变化规律, 并建立了材料的划痕硬度、屈服强度、努氏硬度等参数之间的关系.

2 实验过程

为研究不同种类材料在仪器化划入过程的行为, 选取了3种高分子和20种金属, 共计23种典型广泛应用的工程韧性材料, 材料组织结构致密, 性能均匀, 内部无缺陷, 弹性模量E和屈服强度σ_y列于表1[56–84]. 努氏硬度测试使用钜晶MHVKD-100硬度计, 载荷为100 gf (gf为克力, 表示1 g物体所受重力, 克力值乘地球重力加速度9.8 m/s^2可转换为单位为m N的载荷值), 保载时间为15 s, 5次实验的平均值作为努氏硬度H_K, 也列于表1. 实验前, 用耐水砂纸对材料进行多级水磨, 随后进行机械抛光直到镜面效果肉眼可见, 试样表面在金相

表 1 23种材料力学性能参数

Table 1 Mechanical properties of 23 materials

Materials	E (GPa)	σ_y (MPa)	H_K (GPa)	E/H_K
PC	2.9[56]	70[57]	0.15	19.3
PMMA	3.3[58]	90[58]	0.21	15.7
POM	2.6[59]	40[60]	0.16	16.3
Mo	320[61]	348[62]	3.25	98.5
H59	98[63]	300[64]	1.56	62.8
H62	105[65]	240[66]	1.43	73.4
AZ31	43.8[67]	94[68]	0.73	60.0
AZ41	42[65]	184[65]	0.72	58.3
AZ61	41.5[69]	200[67]	0.86	48.3
Q235	208[43]	235[70]	2.07	100.5
W18Cr4V	210[71]	422[71]	2.86	73.4
65Mn	211[71]	490[72]	3.05	69.2
60Si2Mn	206[71]	1180[70]	3.42	60.2
QT500	151-160[73]	350[74]	2.01	77.1
40Cr	211[71]	1080[75]	2.88	73.3
20#	223[76]	280[77]	1.67	133.5
Al-Si	100[78]	475[78]	2.62	38.2
T8	203[71]	290[79]	2.35	86.4
T10	200[71]	319[80]	2.43	82.3
T12	200[71]	265[71]	2.69	74.3
GCr15	223[81]	353[70]	2.37	94.1
HT150	116[82]	120[82]	2.24	51.8
Fe	217[83]	142[84]	2.11	102.8

显微镜下观察不到划痕, 然后依次在丙酮、无水乙醇和超纯水中进行10 min的超声清洗, 除油去污, 最后用高纯氮气吹干后放入干燥恒温箱中密封保存备用. 利用FEI Quanta TM250环境扫描电子显微镜(SEM)对Al-Si合金表面进行背散射电子(Back Scatter Electron, BSE)成像, 并对Al和Si元素进行能谱(Energy Dispersive Spectrometer, EDS)分析.

划痕测试使用Anton Paar公司的MST^{2}型微米划痕仪, 球形氧化锆陶瓷压头的半径为R = 500 μm, 划痕长度l = 5 mm, 水平速度v = 5 mm/min, 采用渐进的法向载荷F_n, 实验时F_n从5 mN线性增加到25 N. 仪器化划入实验分4步: (1) 压头在很小的法向载荷(5 mN)下对试样表面进行预扫描(pre-scan), 获得试样表面初始轮廓高度; (2) 压头回到扫描起点, 以恒定速度v在试样表面直线滑动, 同时法向载荷F_n线性增大, 同步记录侧向力F_t、压头法向位移等信息, 在试样表面刻划出一条沟槽, 并根据压头的垂直位移与初始轮廓高度的差值得到材料的真实压入深度d_p; (3) 压头再回到扫描起点, 以很小的法向载荷(5 mN)进行后扫描(post-scan), 由压头的垂直位移与初始轮廓高度的差值得到划痕的残余深度d_r; (4) 由仪器自带的光学显微镜对划痕形貌进行多景深的全景成像.

3 结果与分析

4种典型材料的划痕光学形貌如图1所示. 图1(a)是高分子PC的划痕光学形貌: 当F_n较小时, PC主要发生弹性变形, 划痕轮廓很微弱; 随着F_n的增大, 塑性变形增大, 划痕边缘光滑且清晰可见; 微孔洞(Micro holes)的出现是由于压头后面的材料承受拉应力, 且微孔洞分布在划痕的白色区域上, 这是应力白化(Stress-Whitening)现象[85,86]; 微小的划槽(Micro Groove)的出现是由于从微孔洞中脱出的碎屑会随着压头移动与基体材料之间形成三体磨损[87]. 图1(b)是镁合金AZ41的划痕形貌: 因为多晶体AZ41的晶向之间的差异会影响材料的局部变形行为[54], 因此造成划痕两侧的塑性变形有差异, 同时在划痕过程中会形成孪晶现象(Twin Crystal)[88], 此外, 压头顶部对材料表面的摩擦力会拖动位于压头后面的材料, 使得压头后面材料承受拉应力, 压头前面材料承受压应力[89,90], 使得划痕表面出现垂直于划痕方向的裂纹(Cracking). 图1(c)是黄铜

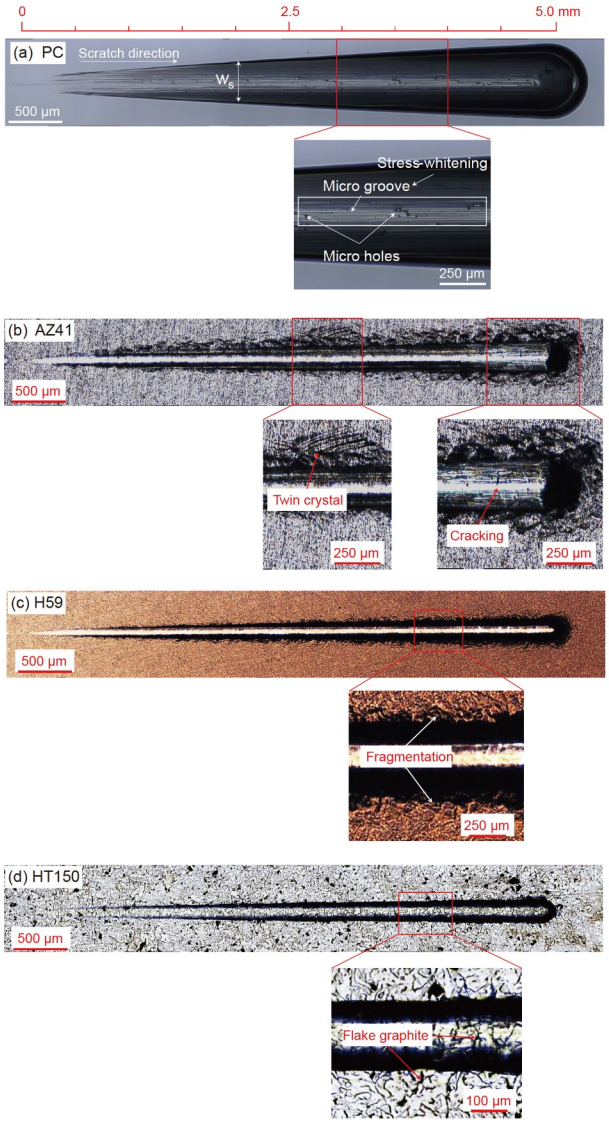


图 1 (网络版彩图)残余划痕的光学图像. (a) PC, (b) AZ41, (c) H59, (d) HT150 (Micro holes-微孔洞; Stress-whitening-应力白化; Micro groove-微小的划槽; Twin crystal-孪晶现象; Cracking-裂纹; Fragmentation-脆性破裂; Flake graphite-片状石墨)

Figure 1 (Color online) Optical images of morphologies of residual scratch. (a) PC, (b) AZ41, (c) H59, (d) HT150.

H59的划痕形貌: 划痕边缘有脆性破裂(Fragmentation)现象, 使划痕轮廓出现锯齿形波动, 这是由材料的剪切流动和撕裂引起的[19], 导致侧向力发生振荡, 引起摩擦系数的波动[91], 随载荷增大, 破裂加剧. 图1(d)为灰口铸铁HT150的划痕形貌图: 划痕边缘较光滑, 沟槽内部可以清晰看到片状石墨(Flake Graphite). 4种材料的划痕形貌差异很大, 表明不同种类材料之间的摩擦行

为存在差异. 压头划刻过程中产生的剪切应力是导致材料变形的主要因素[47].

材料的表面粗糙度会在微观摩擦中起重要作用[92], 使压头与材料在接触和滑移过程中同时存在黏着摩擦力和犁沟摩擦力[93]. 黏着摩擦力来源于小载荷下, 压头与材料表面在接触应力作用下形成的“冷焊”接触点, 对应黏着摩擦系数; 而大载荷下, 压头会在材料表面犁耕出一条沟槽, 此时, 材料抵抗压头犁耕的力就是犁沟摩擦力, 与之对应的是犁沟摩擦系数. 当载荷较小时, 材料主要发生弹性变形, 压头与材料间的接触为赫兹接触, 黏着摩擦在划痕中起主要作用; 随载荷增大, 压入深度增加, 材料表面出现划槽, 犁耕作用显著, 黏着摩擦逐渐过渡到犁耕摩擦, 此时, 由于被压头犁耕出的材料会堆积在压头前端形成阻碍作用, 造成摩擦系数的迅速增加. 在大载荷下, 材料产生明显的塑性变形, 说明随着载荷增加的摩擦系数, 主要是以犁耕摩擦系数为主.

图2(a)和(b)比较了6种典型材料的摩擦系数μ (= F_t/F_n, 即侧向力F_t与法向载荷F_n的比值[28])随法向载荷F_n的变化. 摩擦系数的变化意味着磨损机制的改变[94], 金属材料的摩擦系数随载荷增大出现小幅度的波动, 而高分子的摩擦系数变化较为平滑, 这是因为金属材料摩擦系数受到晶界和晶体取向的影响[95]. 灰口铸铁HT150的摩擦系数随载荷增大先减小后趋于平稳; 高速钢W18Cr4V和碳素钢Q235的摩擦系数随载荷增加而非线性增大, 其余金属材料也呈现相同的趋势. 小载荷下灰口铸铁HT150摩擦系数有下降趋势, 这是由于随法向载荷的增大, 压头与材料间的接触面积增大, 压头与片状石墨(如图1(d))的接触概率增加, 压头与石墨形成的石墨膜的润滑作用导致摩擦系数下降; 随载荷的增大, 压头与材料间发生的粘滑运动[96]占主导, 压入深度的增大使得压头穿透石墨膜而接触铸铁基体, 引起石墨膜的破裂, 摩擦系数不再减小, 最终石墨膜的润滑和黏滑运动达到平衡, 使得摩擦系数趋于平稳. 球墨铸铁QT500与灰口铸铁HT150的摩擦系数呈现同样的变化趋势.

图3(a)和(b)显示3种典型金属的侧向力分别随载荷和压入深度的变化. F_t随F_n的增加而非线性增大, 其余20种材料的侧向力有相同的变化趋势. 碳素结构钢T8, T10和T12中碳含量逐渐增加, 造成材料组织中硬而脆的二次渗碳体含量增加, 使得T8, T10和T12的硬度逐渐增大, 见表1的努氏硬度H_K. 虽然三种碳素结构钢的努氏硬度H_K相差较小, 但是T8的侧向力却与T10和T12差别很大, T8钢的侧向力最大, 这说明材料的抗划擦性能受到多种因素影响, 不能用硬度一种参数简单衡量材料的抗划擦性能. 材料的E/H_K值越大, 材料在摩擦过程中的犁耕作用就越强[97]. 相比于T10和T12钢, T8钢E/H_K (= 86.4, 见表1)最大, 犁耕作用最强, 使得材料对压头阻碍作用最强, 侧向力F_t最大.

图4为压入深度d_p随法向载荷F_n的变化趋势: 随F_n的增大, d_p非线性增大, 且与F_n满足幂律关系. 采用Berkovich压头得到的d_p与F_n也满足幂律关系[98]; 而使用锥角是120°的Rockwell C压头对金属材料进行划痕实验发现, d_p随法向载荷的增大线性增大[99], 表明压头

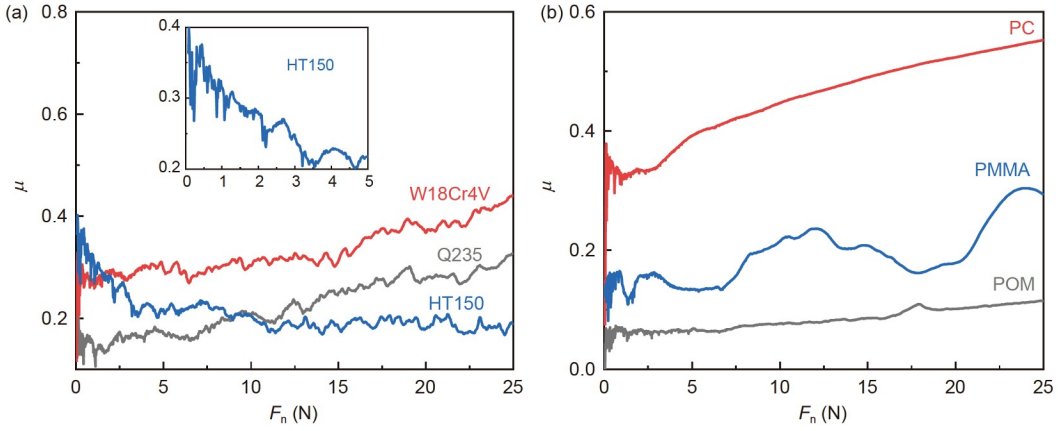


图 2 (网络版彩图)摩擦系数μ随法向载荷F_n的变化. (a) 3种典型金属(插图展示了F_n<5 N灰口铸铁HT150的μ); (b) 3种高分子

Figure 2 (Color online) Variation of friction coefficient μ with normal load F_n for (a) 3 typical metals (inset shows μ of grey cast iron HT150 when F_n<5 N), and (b) 3 polymers.

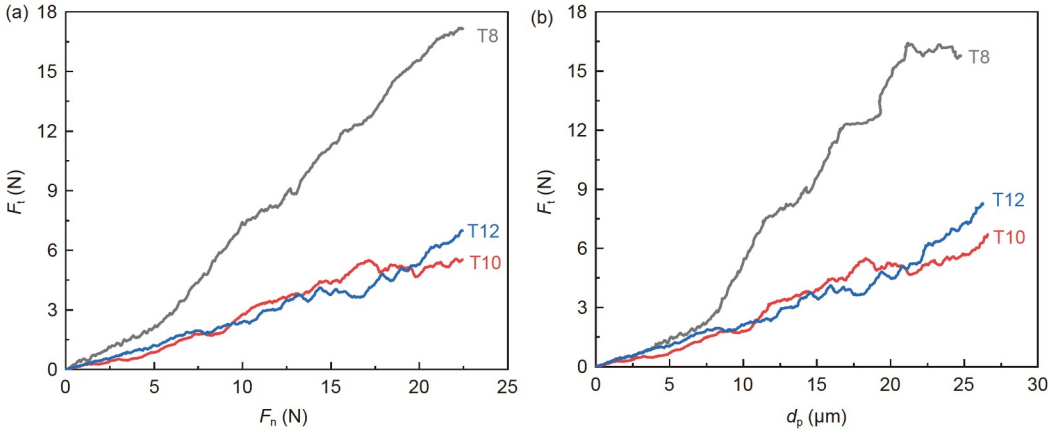


图 3 (网络版彩图) 3种典型金属的侧向力F_t随法向载荷F_n (a)以及压入深度d_p (b)的变化

Figure 3 (Color online) Variation of lateral force F_t of 3 typical materials with (a) normal load F_n and (b) penetration depth d_p.

形状对划痕响应的重要影响. 当载荷较小时(F_n < 1 N), 虽然Mo的硬度(H_K = 3.25 GPa)远大于AZ61的硬度(H_K = 0.72 GPa), 但是它们的d_p差别不大; 而PC的硬度很小(H_K = 0.15 GPa), d_p远大于Mo和AZ61. 这说明小载荷下材料的弹塑性变形都很显著, 单纯的硬度指标不能用来预测划痕过程中的抗压入能力. Khruschov等人[100]的研究表明, 金属耐磨性的提高还取决于金属的硬化方式(合金化、热处理或者加工硬化), 合金中组织的存在使得其磨损机制和纯金属的磨损机制存在差异性, 所以镁合金AZ61和纯金属Mo在划痕中剪切变形存在不同机制.

弹性回复率φ可以衡量材料的弹性变形在总变形

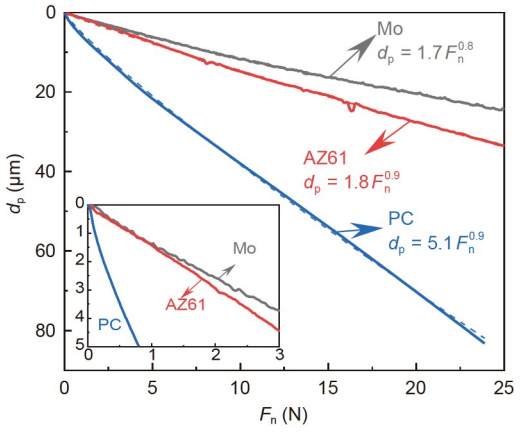


图 4 (网络版彩图) 3种典型材料压入深度d_p与法向载荷F_n的关系(插图比较了F_n<3 N的d_p)

Figure 4 (Color online) Variation of penetration depth d_p with normal load F_n for 3 typical materials (inset compares d_p when F_n < 3 N).

量中所占的比例[47,101]:

$$\varphi = \frac{d_p - d_r}{d_p} \times 100\%, \tag{1}$$

式中, 压入深度d_p代表材料的总变形量, 残余深度d_r是材料的塑性变形量, $d_p - d_r$表示弹性变形量, 当φ大于50%时, 材料以弹性变形为主; 当φ小于50%时, 塑性变形占主导. 在圆球压头划痕实验中, 常用$\varepsilon = d_p/R$表示划痕应变[102], 六种典型材料的弹性回复率φ随ε的变化如图5所示. 所有材料的弹性回复率: 50% < φ < 100%, 说明在圆球压头的作用下弹塑性变形在整个划痕过程中都有显著作用. 当F_n较小时, 试样主要以弹性变形为主, 材料与压头的接触可视为赫兹接触[103], 压头与材料间有一定的黏附作用, 其黏附强度与材料剪切应力有关[104], 此时弹性回复率接近100%. 随着F_n不断增大, 弹性变形减少而塑性变形增加, 弹性回复率减小. 在很大的载荷下, 除了Mo以外的所有金属, 弹性回复率趋近于恒定, 说明材料的弹性塑性变形比已趋于稳定; 然而对于高分子材料, 弹性回复率持续下降, 需要更大的载荷才能到达稳定阶段. 载荷足够大时, 尖锐的棱锥压头使得摩擦机制由犁耕摩擦过渡到切削摩擦, 此时弹性回复率趋近为恒定值[103]. 然而对于圆球压头, 切削摩擦可以忽略, 在大载荷下, 弹性变形与塑性变形竞争机制达到平衡, 导致恒定的弹性回复率. 金属Mo的弹性回复率随着F_n的增大一直增加, 这主要是因为Mo的加工硬化作用很显著, 材料强度的提高造成弹性回复率增大, 这与后面图中Mo的几何划痕硬度随载

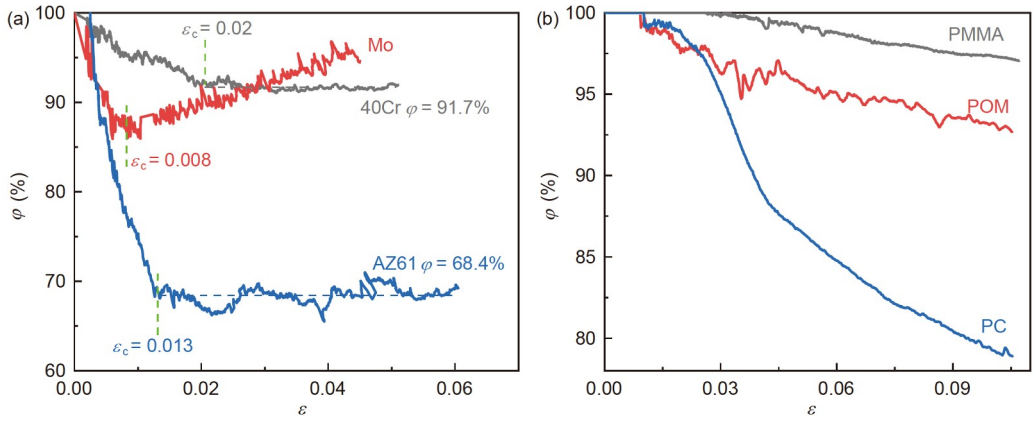


图 5 (网络版彩图)划入过程中弹性回复率φ随划痕应变ε的变化. (a) 3种典型金属; (b) 3种高分子

Figure 5 (Color online) Variation of elastic recovery rate with scratch strain ε during scratching of (a) 3 typical metals and (b) 3 polymers.

荷的增大持续增大相一致. 材料在稳定阶段的弹性回复率列于表2. 高分子材料和Mo在现有载荷下未达到稳定阶段. 较大的弹性回复率可以有效减小划痕在材料表面的可见性[105], 65Mn的弹性回复率很大, 所以抗划擦性能较好. AZ31的弹性回复率较小, 可以预测其在微切削加工中的切削效率较高. 随压头压入深度的增加, 弹性回复率在某个临界划痕应变ε_c下会发生转变, 比如Mo的弹性回复率随应变的增大先减小后增大, φ在最小值时对应的应变就是Mo的临界划痕应变; 大部分的金属材料弹性回复率随ε的增加先减小后趋于平稳, ε_c就是φ平稳阶段的起始应变. 屈服强度与杨氏弹性模量的比值σ_y/E为屈服应变[106,107], σ_y/E越小, 表明材料越早进入到稳定的弹塑性变形阶段.

划痕宽度的两种测量方式: 一种是使用图像处理软件Gwyddion[108]通过量取划痕的光学图像, 见图1, 得到残余划痕宽度w_s; 另一种是根据压头与材料的几何接触模型, 见图6(a)和(b), 计算得到几何划痕宽度w_c[16]:

$$w_c = 2\sqrt{d_p\left(2R - d_p\right)}. \tag{2}$$

划痕硬度常用于量化材料的抗划擦能力[109], 但是当表面出现较为复杂的失效模式时(比如表面裂纹, 剥层等现象), 划痕硬度无法有效衡量损伤程度, 存在一定的局限性[110]. 划痕硬度在一定程度上会受到压头形状[111]、划痕速度[102]、加工硬化程度[112]、表面粗糙度及尺寸效应的影响[113,114]. 较高的划痕硬度能够更好地抵抗外力对表面的划刻, 同时降低磨损率[115]. 假设

表 2 材料的弹性回复率和硬度

Table 2 Scratch hardness and elastic recovery rate of materials

Materials	H_{sa} (GPa)	H_{ca} (GPa)	H_{ta} (GPa)	φ (%)
PC	0.16	–	0.44	–
PMMA	0.47	–	0.25	–
POM	0.32	–	0.09	–
Mo	2.85	–	1.10	–
H59	1.11	0.54	0.87	89.3
H62	0.98	0.60	1.06	88.1
AZ31	0.63	0.36	0.38	72.1
AZ41	0.69	0.39	0.60	75.0
AZ61	0.72	0.48	0.92	68.4
Q235	1.46	0.65	1.53	84.4
W18Cr4V	1.73	0.67	2.15	88.3
65Mn	2.86	0.63	1.59	92.4
60Si2Mn	2.88	0.64	–	92.1
QT500	1.87	0.58	–	86.6
40Cr	2.76	0.61	0.88	91.6
20#	2.03	0.59	0.80	84.8
Al-Si	0.47	0.54	3.19	75.9
T8	1.51	0.57	1.39	88.3
T10	1.83	0.60	1.15	90.6
T12	2.02	0.61	1.33	90.9
GCr15	1.29	0.62	1.34	88.6
HT150	1.07	0.50	0.97	82.2
Fe	1.05	0.60	1.43	83.2

法向投影面积是个半圆, 残余划痕硬度H_s可以由残余划痕宽度w_s计算, 几何划痕硬度H_c可以由几何划痕宽

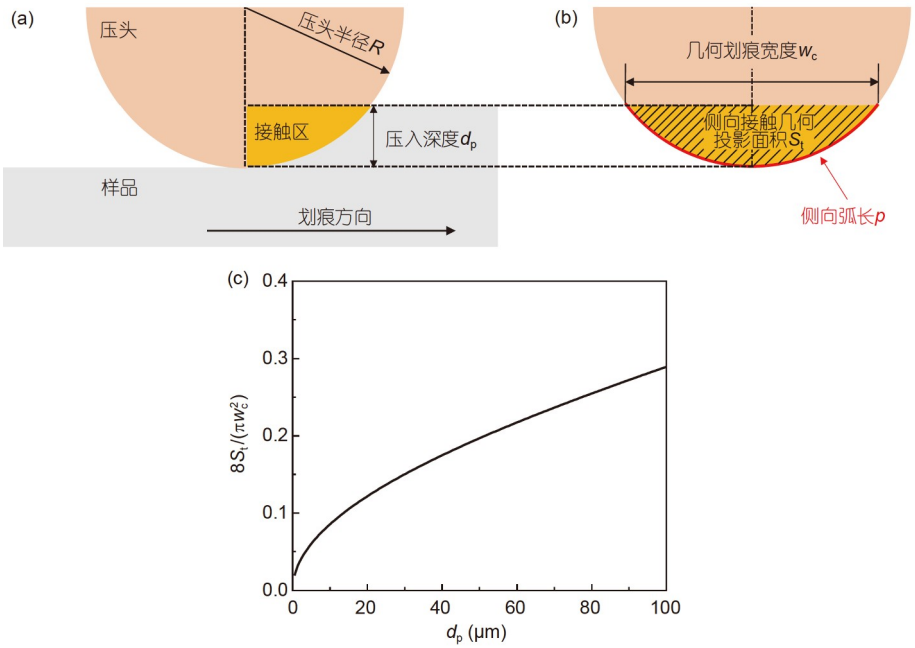


图 6 (网络版彩图)压头与材料几何接触示意图. (a) 主视图; (b) 侧视图; (c) $8S_t/(\pi w_c^2)$与d_p的关系

Figure 6 (Color online) Schematic diagram of geometric contact between indenter and material. (a) Front view; (b) side view; (c) $8S_t/(\pi w_c^2)$ vs. d_p.

度w_c计算. 侧向划痕硬度H_t可以由侧向力除以侧向接触几何投影面积S_t得到, 如图6(a)和(b)所示. 三种划痕硬度的计算公式如下[116]:

$$H_s=\frac{8F_n}{\pi w_s^2},H_c=\frac{8F_n}{\pi w_c^2},H_t=\frac{F_t}{S_t},$$
$$S_t=\frac{1}{2}pR-\left(R-d_p\right)\sqrt{R^2-\left(R-d_p\right)^2},\quad(3)$$
$$p=2R\cos^{-1}\left(\frac{R-d_p}{R}\right),$$

式中, p为球形压头与材料接触时的侧向弧长.

若H_c和H_t相等, 见后面的结果, 则摩擦系数μ还可根据式(3)表示为

$$\mu=\frac{F_t}{F_n}=\frac{H_tS_t}{H_c\pi w_c^2/8}=\frac{8}{\pi}\frac{S_t}{w_c^2},\quad 当\ H_c=H_t时,\quad(4)$$

式中, S_t和w_c^2均为划入深度d_p的函数, 则μ亦为d_p的函数. 图6(c)为$8S_t/(\pi w_c^2)$与d_p的关系: 当$H_c=H_t$, $8S_t/(\pi w_c^2)$随d_p的增大而增大, 由于d_p随F_n的增大而非线性增大, 见图4, 可以得出μ随F_n的增大而非线性增大, 见图2, 所以摩擦系数的持续增大是由于球形压头几何形状的影响. 灰口铸铁HT150和球墨铸铁QT500的μ最后趋于稳定是由于石墨的影响.

图7显示了2种典型材料的残余划痕宽度w_s的平方随F_n的变化: 在小载荷下, w_s的平方与F_n的关系可以用幂函数来表示; 对于金属材料, 即使在小载荷下, w_s的平方与F_n也近似呈线性关系; 只是高分子材料在小载

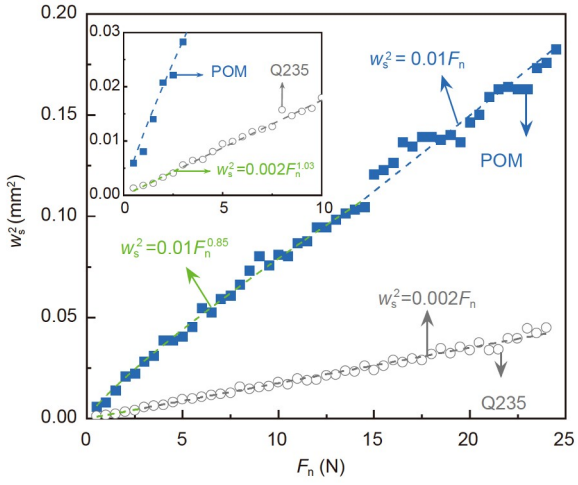


图 7 (网络版彩图)两种典型材料的残余划痕宽度w_s的平方随法向载荷F_n的变化(插图展示了F_n<10 N的w_s)

Figure 7 (Color online) Variation of square of residual scratch width w_s with normal load F_n for 2 typical materials (inset shows w_s when F_n < 10 N).

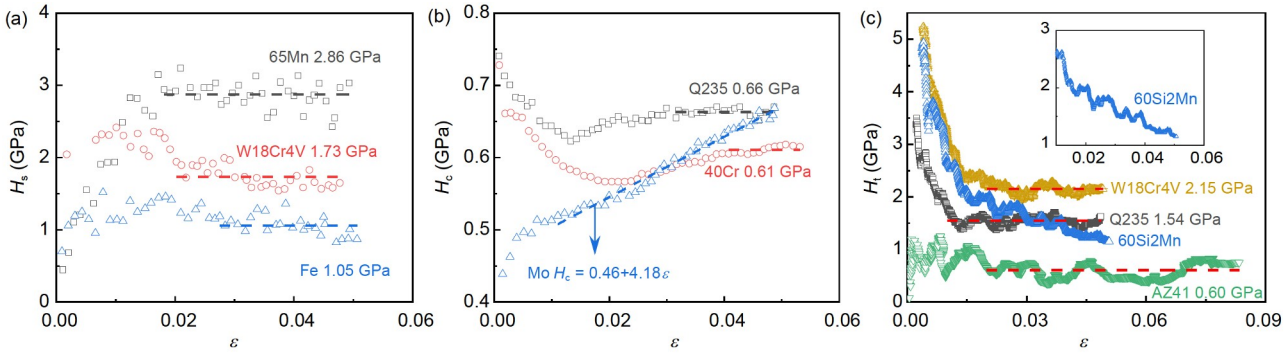


图 8 (网络版彩图)典型金属材料的(a) H_s, (b) H_c和(c) H_t随ε的变化(插图展示了60Si2Mn的H_t)

Figure 8 (Color online) Variations of (a) H_s, (b) H_c, and (c) H_t with ε for typical metal materials (inset shows H_t of 60Si2Mn).

荷下偏离线性关系较远; 在大载荷下, w_s的平方与F_n呈线性关系; 说明残余划痕硬度H_s在大载荷下会趋于常数, 这与Wong等人[86]的实验结论一致.

图8显示残余划痕硬度H_s、几何划痕硬度H_c和侧向划痕硬度H_t随ε的变化. 所有材料的残余划痕硬度H_s在较大的应变下都会趋于稳定. 金属材料(Mo除外)的几何划痕硬度H_c在较大的应变下也会趋于稳定. Mo的几何划痕硬度一直增加, 并且与应变d_p/R有线性关系. 对于硬度较小的高分子以及硬度极大的Mo, 几何划痕硬度都无法趋于常数, 可能是因为载荷太小, 稳定的塑性变形阶段还未达到. 只有一部分材料的侧向划痕硬度在较大的应变下会趋于稳定; 即使对于某些金属材料(比如60Si2Mn), H_t随ε的增大持续下降, 没有平稳阶段. H_s, H_c和H_t在较大应变下的稳定值H_{sa}, H_{ca}和H_{ta}列于表2. 室温下, 黄铜H59和H62都是由(α + β)相组成的双相黄铜, α相的塑形性能好, β相硬度较大, 且β相会随着锌含量的增加而变多[117], 因此, 锌含量较多的H59的强度更高, 使得H59残余划痕硬度H_{sa} (1.11 GPa)大于H62 (0.98 GPa). 对于镁合金, 随着Al含量的增加, AZ31, AZ41和AZ61的残余划痕硬度H_{sa}逐渐增大, 这是因为这三种镁合金由α-Mg固溶体和β-$Mg_{17}Al_{12}$金属间化合物组成[118], 由于Al元素有较强固溶强化作用, Al元素含量的增加使得位于晶界上的β-$Mg_{17}Al_{12}$对晶界的钉扎作用增强, 并抑制晶界的转动作用, 使得镁合金的强度不断提高, 所以AZ61 (含铝最多)的残余划痕硬度H_{sa}最大, AZ31 (含铝最少)的残余划痕硬度最小, 但是Al含量的增加同时会使β-$Mg_{17}Al_{12}$金属间化合物增多而形成过厚的晶界, 导致镁合金的韧性降低[119]. 材料的划痕硬度取决于材料在划入过程中的抗变形能力, 较高的弹性模量和致密化有利于提高材料的抗划擦性[120], 对致密化较高的材料, 载荷增加无法再压缩材料, 会促进剪切变形的发展[121].

根据线弹性断裂力学(LEFM)理论可以计算平面应变断裂韧度K_C[28]:

$$K_C = \frac{F_t}{\sqrt{2pS_t}}. \tag{5}$$

三种高分子材料(PC, PMMA, POM)基于LEFM理论的断裂韧度分析如图9所示. 需要足够大的载荷才能产生稳定扩展的裂纹, 最大载荷下计算得到的断裂韧度值(图中水平虚线)与文献中的结果一致(PC和PMMA的断裂韧度值分别为2.2[122]和1.5 MPa $m^{1/2}$[123]), POM的断裂韧度为0.5 MPa $m^{1/2}$.

图10(a)比较了20种金属材料的临界划痕应变ε_c与

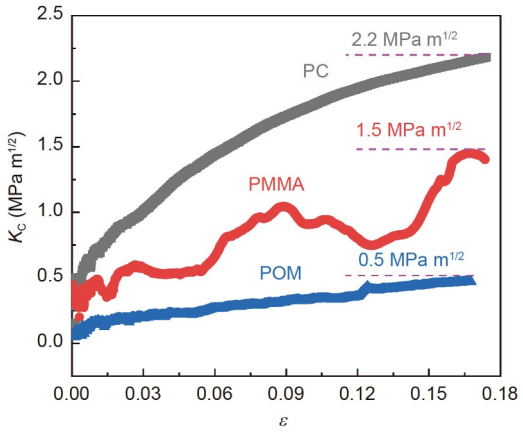


图 9 (网络版彩图)三种高分子材料的断裂韧度K_C随ε的变化

Figure 9 (Color online) Variations of fracture toughness K_C with ε for 3 polymers.

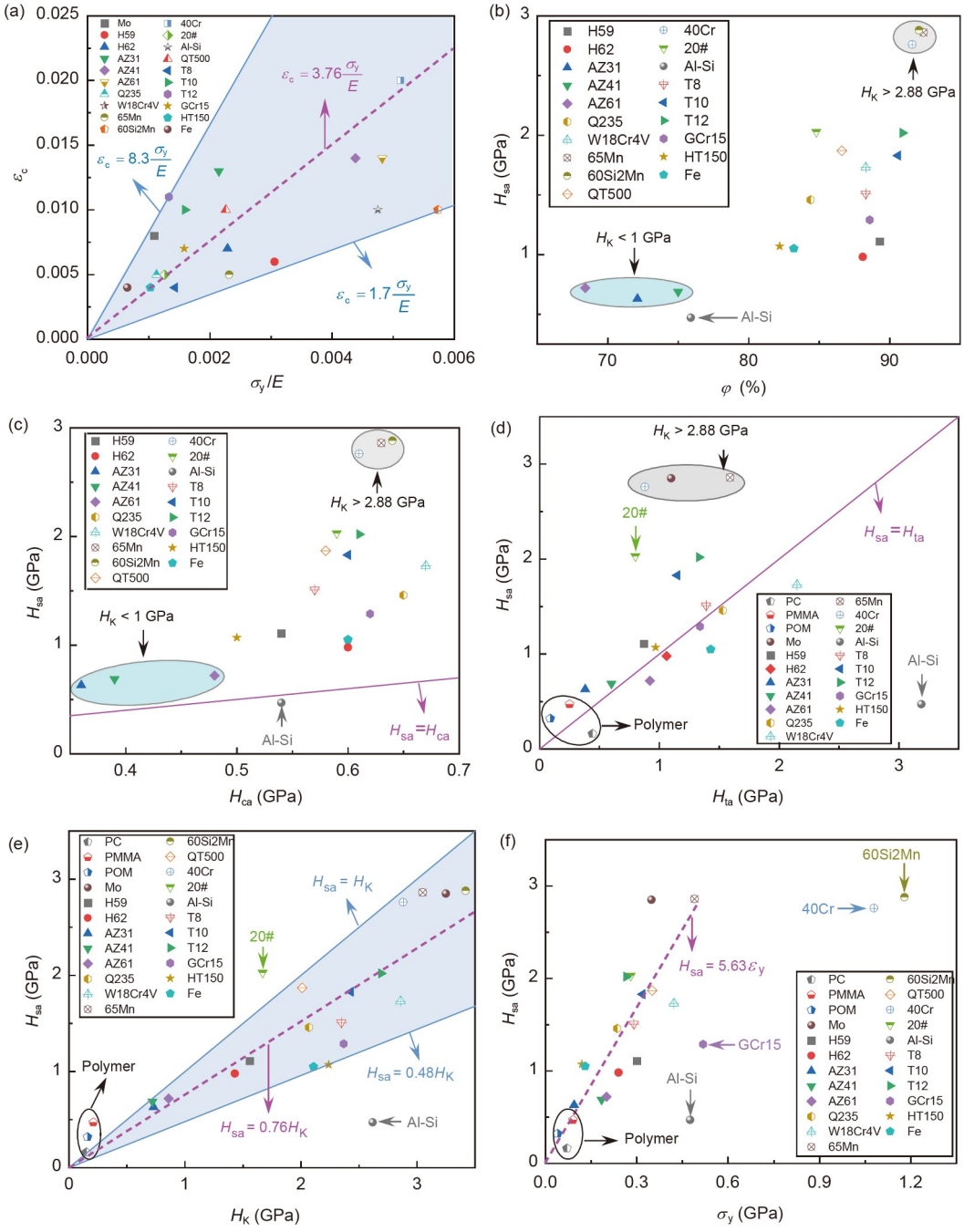


图 10 (网络版彩图) H_{sa}, φ, ε_c, H_{ca}, H_{ta}, H_K, σ_y和E之间的关系. (a) ε_c与σ_y/E; (b) H_{sa}与φ; (c) H_{sa}与H_{ca}; (d) H_{sa}与H_{ca}; (e) H_{sa}与H_K; (f) H_{sa}与σ_y

Figure 10 (Color online) Relationships among H_{sa}, φ, ε_c, H_{ca}, H_{ta}, H_K, σ_y and E. (a) ε_c vs. σ_y/E; (b) H_{sa} vs. φ; (c) H_{sa} vs. H_{ca}; (d) H_{sa} vs. H_{ca}; (e) H_{sa} vs. H_K; (f) H_{sa} vs. σ_y.

屈服应变σ_y/E的关系, 对数据进行线性拟合发现ε_c = 3.76σ_y/E, 比例系数在1.7–8.3之间, 表明仪器化划入方法得到的结果可以作为金属材料的弹塑性性能的参照; 虽然大体上ε_c有随σ_y/E的增大而增大的趋势, 但是ε_c与σ_y/E没有简单的关系, 这说明金属材料塑性屈服之后的硬化行为对划入过程有显著影响. 图10(b)比较了

稳定残余划痕硬度H_{sa}与稳定弹性回复率φ之间的关系(3种高分子和Mo的φ无稳定阶段, 没有考虑). 对于努氏硬度较小的AZ系镁合金, φ相对较小, 塑性变形能力更强; 努氏硬度较大的硬金属, 如65Mn, 40Cr和60Si2Mn的H_{sa}和φ均较大, 这是因为材料的屈服强度及弹性模量均较大时, 不容易产生塑性变形, 弹性回复更大, 稳定残余划痕硬度H_{sa}也会更大. 图10(c)显示了H_{ca}与H_{sa}之间的关系. 材料的H_{sa}大于H_{ca} (Al-Si合金除外), 这是因为材料被划刻过程中受到了包辛格效应(Bauschinger Effect)影响, 背应力(Back Stress)阻碍位错开动从而抑制了部分滑移系的开动[124], 进而产生的加工硬化[125]抑制了材料的塑性变形[126,127], 使得横向弹性回复能力增强, 导致残余划痕宽度会比几何划痕宽度小. 努氏硬度越小的软金属(如AZ系镁合金), 塑性变形能力更强, 弹性回复较小, 使得残余划痕宽度与几何宽度近似相同, 其残余划痕硬度H_{sa}和几何划痕硬度H_{ca}就越接近; 努氏硬度和弹性模量较大的硬金属(如65Mn, 40Cr和60Si2Mn), 残余划痕硬度远大于几何划痕硬度, 这是因为当屈服强度及弹性模量均较大时, 不容易产生塑性变形, 弹性回复更大, 用几何法计算得到的几何划痕宽度大于残余划痕宽度. 努氏硬度较大的硬金属(如65Mn, 40Cr和60Si2Mn), 稳定残余划痕硬度H_{sa}大于稳定侧向划痕硬度H_{ta}, 见图10(d); 其余大部分材料的H_{sa}与H_{ta}大体相同(Al-Si合金和20#钢除外). 除20#钢和高分子材料外, 材料的残余划痕硬度H_{sa}均小于努氏硬度H_K ($0.48 < H_{sa}/H_K < 1$), H_{sa}与H_K大体上呈正比($H_{sa} = 0.76H_K$), 见图10(e), 这可能是由于划入测试的最大加载力远大于努氏硬度的加载力100 gf; H_{sa}有随H_K增大而增大的趋势, 但是也有例外, 比如, 高速钢W18Cr4V的H_K大于球墨铸铁QT500, 但两者的H_{sa}大小关系却相反, 这主要是因为球磨铸铁中石墨的影响.

图10(f)为材料的屈服强度σ_y和稳定残余划痕硬度H_{sa}间的关系. 大部分金属材料(Al-Si合金, GCr15, 40Cr和60Si2Mn除外)的稳定残余划痕硬度H_{sa}和屈服强度σ_y成比例, 这是因为硬度和强度都是材料在外力作用下抵抗变形和破坏的反映, 硬度和屈服强度的比值与材料的弹性模量[128,129]、应变硬化指数[130]和泊松比[131]等参数有关. 圆球划入测试得到的$H_{sa}/\sigma_y = 5.63$, 大于压入硬度与屈服强度的比值(一般在3左右)[132]. Kurkcu等人[133]研究高分子划痕行为时, 发现残余划痕硬度与屈服强度呈线性关系, 但是Zhu等人[102]的研究表明划痕速度的改变会引起局部应变率波动, 进而影

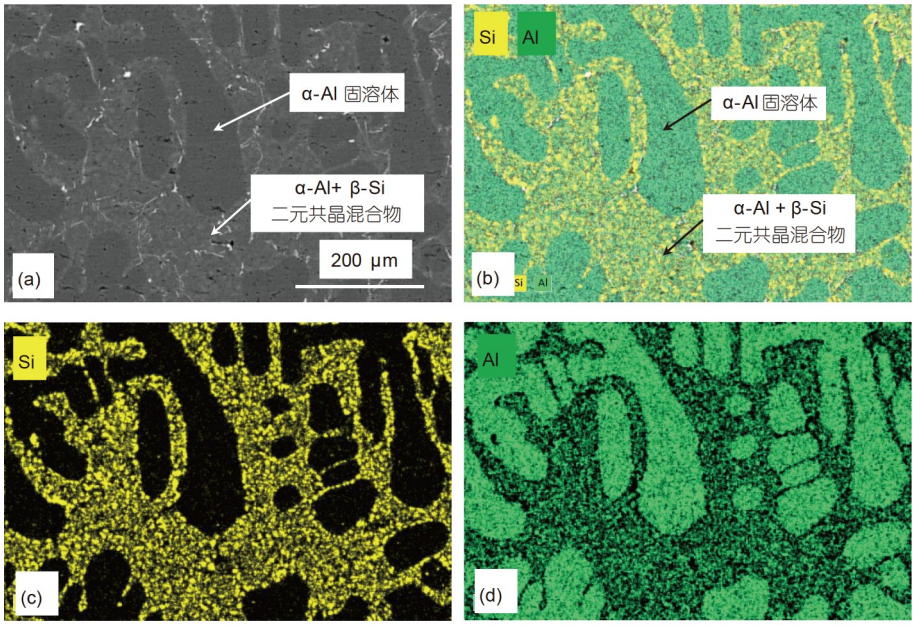


图 11 (网络版彩图) AlSi合金的SEM/EDS面扫描结果. (a) 选定区域的背散射电子成像; (b) Si和Al元素的分布; (c) Si元素分布; (d) Al元素分布

Figure 11 (Color online) SEM/EDS map of AlSi alloy. (a) BSE image of selected area; (b) distribution of Si and Al elements; (c) distribution of Si element; (d) distribution of Al element.

响材料的弹塑性变化及H_{sa}.

Al-Si合金的力学性能对划入响应的影响不同于金属合金的规律, 这是由于脆性的非金属元素Si的影响, 并且其微观组织也很特殊: Al-Si合金主要由α-Al固溶体枝晶和(α-Al + β-Si)二元共晶混合物组成, 见图11. 图11(a)利用扫描电子显微镜(SEM)的背散射电子(BSE)成像可以清楚地区分α-Al固溶体和(α-Al + β-Si)二元共晶混合物, 结合图11(b)–(d)的能谱分析(EDS), 发现非金属元素Si分布较广, 对Al-Si合金的力学性能和变形有重要影响.

4 结论

使用球形压头对常见工程韧性材料(20种金属和3种高分子)在渐进载荷下进行仪器化划入实验, 揭示了划入各种响应参数等随法向载荷的变化规律, 发现金属材料的临界划痕应变(弹性回复率平稳阶段的起始应变, 高分子材料没有临界划痕应变)与屈服应变成正比, 表明仪器化划入结果可以反映金属材料的弹塑性参数; 大部分材料的摩擦系数随着载荷的增大而非线性增长, 主要是球形压头的几何形状导致的, 而灰口铸铁HT150和球墨铸铁QT500的平稳段是由于石墨的影响; 随正压力的增加, 金属的弹性回复率、残余划痕硬度、几何划痕硬度和侧向划痕硬度均趋近于稳定, 说明材料的弹性和塑性变形比已趋于平稳, 然而高分子的弹性回复率、几何划痕硬度和侧向划痕硬度却单调减小, 可能是由于材料发生损伤, 利用线弹性断裂力学方法在最大载荷下计算得到的高分子材料的断裂韧度与文献值相符. 大部分材料的稳定残余划痕硬度与努氏硬度成比例; 大部分材料的稳定残余划痕硬度与屈服强度有线性关系(由于非金属元素β-Si的影响使得Al-Si合金的力学性能对划入响应的影响与其他材料的规律不同), 这是因为硬度和屈服强度可以衡量材料抵抗外力变形的能力. 通过建立划痕硬度、屈服强度和努氏硬度等特征量之间的关系为利用仪器化划入方法表征韧性材料力学性能提供参考和指导.

参考文献

1 Liu M, Wu J N. Scratch behavior of materials under progressive load by conical indenter (in Chinese). Chin J Mater Res, 2022, 36: 191–205 [刘明, 伍家楠. 圆锥压头递增载荷对材料的划痕行为. 材料研究学报, 2022, 36: 191–205]

2 Liu M, Zheng Q, Gao C. Sliding of a diamond sphere on fused silica under ramping load. Mater Today Commun, 2020, 25: 101684

3 Liu M, Wu J, Gao C. Sliding of a diamond sphere on K9 glass under progressive load. J Non-Crystalline Solids, 2019, 526: 119711

4 Liu M, Yan F, Gao C. Influence of sliding velocity on microscratch response of carbohydrate polymers by Berkovich indenter. Polym Test, 2022, 109: 107542

5 Liu M, Wang W. Effects of sliding velocity on microscratch responses of thermoplastics by Berkovich indenter. Polym Bull, 2022, doi: 10.1007/s00289-022-04397-7

6 Liu M, Hou D, Wu L. Influence of poly(ethyleneimine) functionalized multi-walled carbon nanotubes on mechanical and tribological behavior of epoxy resins. Mater Today Commun, 2022, 33: 104480

7 Li S, Zhang J, Liu M, et al. Influence of polyethyleneimine functionalized graphene on tribological behavior of epoxy composite. Polym Bull, 2021, 78: 6493–6515

8 Shu K, Zhang C, Sun D, et al. Contact cracking and delamination of thin solid lubricating films on deformable substrates. Tribol Int, 2021, 163: 107181

9 Ma X, Ma J, Bian X, et al. The role of nano-scale elastic heterogeneity in mechanical and tribological behaviors of a Cu-Zr based metallic glass thin film. Intermetallics, 2021, 133: 107159

10 Liu M, Yan F. Scratch-induced deformation and damage behavior of doped diamond-like carbon films under progressive normal load of Vickers indenter. Thin Solid Films, 2022, 756: 139351

11 Liu M, Li S, Gao C H. Study of failure mechanism of TiN coatings by micro-scratch testing. Acta Metrol Sin, 2020, 44: 696–703

12 Yu J, Tao X F, Qin L, et al. Comparative study on the influence of curvature radius of needle tip on scratch test of hard film bonding force (in Chinese). Acta Metrol Sin, 2020, 41: 1089–1094 [于杰, 陶兴付, 秦林, 等. 压头曲率半径对硬质薄膜结合力划痕测量影响的比较研究. 计量学报, 2020, 41: 1089–1094]

13 Liu M, Liu X J, Gao C H. Microscratch properties of polycarbonate by spherical indenter (in Chinese). Tribology, 2021, 41: 890–901 [刘明, 刘星君, 高诚辉. 利用球形压头研究聚碳酸酯的微米划痕性能. 摩擦学学报, 2021, 41: 890–901]

14 Teisala H, Baumli P, Weber S A L, et al. Grafting silicone at room temperature—a transparent, scratch-resistant nonstick molecular coating. Langmuir, 2020, 36: 4416–4431

15 Sundararajan M, Devarajan M, Jaafar M. A novel sealing and high scratch resistant nanorod Ni-P coating on anodic aluminum oxide. Mater Lett, 2021, 289: 129425

16 Gao C, Liu M. Effects of normal load on the coefficient of friction by microscratch test of copper with a spherical indenter. Tribol Lett, 2019, 67: 8

17 Liu M, Yang S, Gao C. Scratch behavior of polycarbonate by Rockwell C diamond indenter under progressive loading. Polym Testing, 2020, 90: 106643

18 Gao C, Liu M. Effect of sample tilt on measurement of friction coefficient by constant-load scratch testing of copper with a spherical indenter. J Test Eval, 2020, 48: 20180719

19 Liu M. Characterization of bulk metallic glasses by microscratch test under Rockwell C diamond indenter and progressive normal load. Eng Fract Mech, 2023, 281: 109126

20 Liu M, Yan F W, Gao C H. Effect of normal load on microscratch test of copper (in Chinese). Acta Metrol Sin, 2020, 41: 1095–1101 [刘明, 严富文, 高诚辉. 法向载荷对紫铜的微米划痕测试的影响. 计量学报, 2020, 41: 1095–1101]

21 Liu M, Yan F W, Gao C H. Effect of sliding velocity of a spherical indenter on microscratch response of materials (in Chinese). J Fuzhou Univ (Nat Sci Ed), 2021, 49: 473–484 [刘明, 严富文, 高诚辉. 球形压头的滑动速度对材料微米划痕响应的影响. 福州大学学报: 自然科学版, 2021, 49: 473–484]

22 Liu M. Influence of sample tilt and applied load on microscratch behavior of copper under a spherical diamond indenter. Tribol Lett, 2021, 69: 88

23 Liu M, Huang C X, Gao C H. Effect of sample tilt on measurement of friction coefficient by microscratch test of copper with a spherical indenter (in Chinese). Acta Metrol Sin, 2020, 41: 1252–1259 [刘明, 黄承馨, 高诚辉. 试样倾斜对球形压头微米划痕测试紫铜摩擦系数的影响. 计量学报, 2020, 41: 1252–1259]

24 Liu M, Li S, Gao C H. Study of failure mechanism of TiN coatings by micro-scratch testing (in Chinese). Acta Metrol Sin, 2020, 41: 696–703 [刘明, 李烁, 高诚辉. 利用微米划痕研究TiN涂层的失效机理. 计量学报, 2020, 41: 696–703]

25 R M, Bellon P, Averback R S. Wear resistance of Cu/Ag multilayers: A microscopic study. ACS Appl Mater Interfaces, 2018, 10: 15288–15297

26 Liu M, Li G X, Zhou C, et al. Analysis of 3D morphology and scratch hardness o copper under constant big load scratch test (in Chinese). Tribology, 2021, 41: 467–473 [刘明, 李国翔, 周超, 等. 恒定大载荷划痕试验下紫铜的三维形貌及划痕硬度分析. 摩擦学学报, 2021, 41: 467–473]

27 Liu M, Li S, Gao C H. Fracture toughness measurement by micro-scratch tests with conical indenter (in Chinese). Tribology, 2019, 39: 36–44 [刘明, 李烁, 高诚辉. 利用圆锥压头微米划痕测试材料断裂韧性. 摩擦学学报, 2019, 39: 36–44]

28 Liu M, Xu Z, Fu R. Micromechanical and microstructure characterization of BaO-Sm_2O_3-5TiO_2 ceramic with addition of Al_2O_3. Ceramics Int, 2022, 48: 992–1005

29 Zhang D, Sun Y, Gao C, et al. Measurement of fracture toughness of copper via constant-load microscratch with a spherical indenter. Wear, 2020, 444-445: 203158

30 Liu M, Hou D, Gao C H. Study on fracture toughness of semiconductor material using Vickers and Berkovich indenters. Chin J Theor Appl Mech, 2021, 53: 413–423

31 Liu M, Li S, Gao C H. Fracture toughness measurement by micro-scratch tests with conical indenter. Tribology, 2019, 39: 556–564

32 Liu M, Hou D Y, Gao C H. Study on fracture toughness of semiconductor material using Vickers and Berkovich indenters (in Chinese). Chin J Theor Appl Mech, 2021, 53: 413–423 [刘明, 侯冬杨, 高诚辉. 利用维氏和玻氏压头表征半导体材料断裂韧性. 力学学报, 2021, 53: 413–423]

33 Xu Y, Li D, Shen J B, et al. Research progress in scratch behaviors of polymeric materials (in Chinese). Acta Polym Sin, 2018: 1262–1278 [徐杨, 李顿, 沈佳斌, 等. 高分子材料刮擦行为研究进展. 高分子学报, 2018: 1262–1278]

34 Liu M, Yang S H, Gao C H. Surface shape vision measurement for scratch based on level set (in Chinese). Chin J Sci Instrum, 2020, 41: 184–194 [刘明, 杨胜寒, 高诚辉. 基于水平集方法的划痕形状表面视觉测量. 仪器仪表学报, 2020, 41: 184–194]

35 Liu M, Xu Z T, Gao C H. Determination of mechanical properties of microstructure in metals based on grid nanoindentation (in Chinese). J Fuzhou Univ (Nat Sci Ed), 2021, 49: 497–808 [刘明, 徐智通, 高诚辉. 纳米压入法点阵分析金属微观组织力学性能. 福州大学学报: 自然科学版, 2021, 49: 497–808]

36 Zhu G Y, Dong X Y, Gao C H, et al. Effects of sample tilt on Berkovich nanoindentation test of fused silica (in Chinese). Acta Metrol Sin, 2019, 40: 289–294 [朱光宇, 董翔宇, 高诚辉, 等. 试样倾斜对熔融石英硅三棱锥纳米压痕测试的影响. 计量学报, 2019, 40: 289–294]

37 Liu M. Microscratch of copper by a Rockwell C diamond indenter under a constant load. Nanotechnol Precision Eng, 2021, 4: 033003

38 Beake B D, Liskiewicz T W, Smith J F. Deformation of Si(100) in spherical contacts—Comparison of nano-fretting and nano-scratch tests with nano-indentation. Surf Coatings Tech, 2011, 206: 1921–1926

39 Beegan D, Chowdhury S, Laugier M T. Comparison between nanoindentation and scratch test hardness (scratch hardness) values of copper thin films on oxidised silicon substrates. Surf Coatings Tech, 2007, 201: 5804–5808

40 AlMotasem A T, Bergström J, Gåård A, et al. Atomistic insights on the wear/friction behavior of nanocrystalline ferrite during nanoscratching as revealed by molecular dynamics. Tribol Lett, 2017, 65: 101

41 Zhang J, Qin J, Li Y, et al. Extraction of the plastic properties of metallic materials from scratch tests using deep learning. Mech Mater, 2022, 175: 104502

42 Zhang J, Li Y, Zheng X, et al. Determination of plastic properties of surface modification layer of metallic materials from scratch tests. Eng Failure Anal, 2022, 142: 106754

43 Ovaert T C, Kim B R. Estimation of polymer coating scratch tensile strength by nano-indentation, micro-scratch testing, and finite element modeling. In: Proceedings of the World Tribology Congress. New York: American Society of Mechanical Engineers, 2005. 405–407

44 Bellemare S C, Dao M, Suresh S. A new method for evaluating the plastic properties of materials through instrumented frictional sliding tests. Acta Mater, 2010, 58: 6385–6392

45 Belov V K, Gubarev E V, Papshev A V, et al. Development of a scratch test method to determine adhesion and strength properties of coated steel sheets. In: Proceedings of the IOP Conference Series Materials Science and Engineering. Moscow, 2019. 012012

46 Huang L, Lu J, Xu K. Elasto-plastic deformation and fracture mechanism of a diamond-like carbon film deposited on a Ti-6Al-4V substrate in nano-scratch test. Thin Solid Films, 2004, 466: 175–182

47 Xiang C, Sue H J, Chu J, et al. Scratch behavior and material property relationship in polymers. J Polym Sci B Polym Phys, 2001, 39: 47–59

48 Bellemare S C, Dao M, Suresh S. Effects of mechanical properties and surface friction on elasto-plastic sliding contact. Mech Mater, 2008, 40: 206–219

49 Beake B D, Vishnyakov V M, Valizadeh R, et al. Influence of mechanical properties on the nanoscratch behaviour of hard nanocomposite TiN/Si_3N_4 coatings on Si. J Phys D-Appl Phys, 2006, 39: 1392–1397

50 Hara Y, Mori T, Fujitani T. Relationship between viscoelasticity and scratch morphology of coating films. Prog Org Coatings, 2000, 40: 39–47

51 Burnett P J, Rickerby D S. The relationship between hardness and scratch adhesion. Thin Solid Films, 1987, 154: 403–416

52 Akono A-T. Scratch Tests: A New Way of Evaluating the Fracture Toughness of Materials. Dissertation for Doctoral Degree. Chicago: Northwestern University, 2011

53 Zhang Y F, He H T, Yu J X, et al. AFM nanoscrach behaviors of three optical glasses used in ICF (in Chinese). Tribology, 2018, 38: 349–355 [张亚锋, 何洪途, 余家欣, 等. 用于ICF的三种典型光学玻璃的AFM纳米划痕行为研究. 摩擦学学报, 2018, 38: 349–355]

54 Pöhl F, Hardes C, Theisen W. Scratch behavior of soft metallic materials. AIMS Mater Sci, 2016, 3: 390–403

55 Xie Z F, Yu J X, Qian L M. Load effect on the translation of friction mechanism of four materials (in Chinese). J Shanghai Jiangtong Univ, 2009, 43: 1930–1935 [谢祖飞, 余家欣, 钱林茂. 载荷对4种材料摩擦机制转变的影响. 上海交通大学学报, 2009, 43: 1930–1935]

56 Cheng R Q, Han X, Su X, et al. Preparation and mechanicl properties of three carbon-based/polycarbonate nanocomposites (in Chinese). J Shenyang Aerosp Univ, 2022, 39: 27–32 [程荣强, 韩绪, 苏潇, 等. 3种碳基/聚碳酸酯纳米复合材料的制备与力学性能. 沈阳航空航天大学学报, 2022, 39: 27–32]

57 Ma X Z, Wang Y, Wang Y. Experiment of the tensile properties of polycarbonate at different strain rates (in Chinese). Polym Mater Sci Eng, 2009, 25: 131–134 [马新忠, 汪洋, 王宇. 聚碳酸酯拉伸力学性能的应变率相关性实验. 高分子材料科学与工程, 2009, 25: 131–134]

58 Vandeperre L J, Giuliani F, Clegg W J. Effect of elastic surface deformation on the relation between hardness and yield strength. J Mater Res, 2004, 19: 3704–3714

59 Xiong X S. Research on Mechanical Properties and Friction and Wear Performance of Flax Fiber Reinforced POM Composites (in Chinese).

Dissertation for Doctoral Degree. Wuhan: Wuhan University of Technology, 2019 [熊小双. 亚麻纤维增强聚甲醛复合材料力学性能及摩擦磨损特性研究. 博士学位论文. 武汉: 武汉理工大学, 2019]

60 Wang L X, Wang Y Z, Wang D F, et al. Mechanism of the influence of processing conditions on mechanical properties of micro injection molded polyformaldehyde parts (in Chinese). Polym Mater Sci Eng, 2017, 33: 89–94 [王利霞, 王永贞, 王东方, 等. 工艺参数对聚甲醛微注塑制品力学性能的影响机理. 高分子材料科学与工程, 2017, 33: 89–94]

61 李春胜, 黄德彬. 机械工程材料手册. 北京: 电子工业出版社, 2006

62 Kleiser G, Revil-Baudard B, Pasiliao C L. High strain-rate plastic deformation of molybdenum: Experimental investigation, constitutive modeling and validation using impact tests. Int J Impact Eng, 2016, 96: 116–128

63 Zhang S C, Liu C, Liu S, et al. Effects of temperature and strain rate on elastic modular of extruded AZ31 magnesium alloy (in Chinese). Light Alloy Fabr Technol, 2016, 44: 62–65 [张诗昌, 刘纯, 刘升, 等. 温度及应变率对挤压态AZ31镁合金弹性模量的影响. 轻合金加工技术, 2016, 44: 62–65]

64 Nobel C, Hofmann U, Klocke F, et al. Experimental investigation of chip formation, flow, and breakage in free orthogonal cutting of copper-zinc alloys. Int J Adv Manuf Technol, 2015, doi: 10.1007/s00170-015-7749-z

65 Tun K S, Minh N J, Nguyen Q B, et al. Investigation on the mechanical properties of Mg-Al alloys (AZ41 and AZ51) and its composites. Metals, 2012, 2: 313–328

66 Pan X X, Huang P F, Su F. Study on the relationship between acoustic emission signals and mechanical behavior of Q345 steel and H62 brass alloy (in Chinese). J Exp Mech, 2016, 31: 431–439 [潘晓旭, 黄鹏飞, 苏飞. Q345钢和H62黄铜声发射信号及力学行为的关系研究. 实验力学, 2016, 31: 431–439]

67 Hilšer O, Rusz S, Szkandera P, et al. Study of the microstructure, tensile properties and hardness of AZ61 magnesium alloy subjected to severe plastic deformation. Metals, 2018, 8: 776

68 Fan L Q. Effect of the Y on the Microstructure and Mechanical Property of As-Cast AZ31 Magnesium Alloy (in Chiness). Dissertation for Master's Degree. Taiyuan: Taiyuan University of Technology, 2013 [范刘群. Y对铸态AZ31镁合金微观组织及力学性能的影响. 硕士学位论文. 太原: 太原理工大学, 2013]

69 Fan X. Microstructure and mechanical properties of high-carbon pearlitic steel after deformation (in Chiness). Foundry Technol, 2014, 35: 247–249 [樊雄. 高碳珠光体钢形变后的微观组织及力学性能研究. 铸造技术, 2014, 35: 247–249]

70 Wu G C, Xu X J, Wang B, et al. Tensile properties of fully annealed 40Cr steel processed by equal-channel angular pressing (in Chinese). Hot Work Technol, 2010, 39: 16–17, 20 [吴桂潮, 许晓静, 王彬, 等. 完全退火态40Cr钢ECAP加工后的拉伸性能. 热加工工艺, 2010, 39: 16–17, 20]

71 张建军. 机械工程材料. 重庆: 西南师范大学出版社, 2015

72 Li Z T, Luo B, Zhou J X, et al. Development and production practice of 65 Mn hot-rollin strip steel in cheng steel (in Chinese). Hebei Metall, 2015, 2: 33–34 [李正团, 罗波, 周景鑫, 等. 承钢65Mn热轧带钢的开发与生产实践. 河北冶金, 2015, 2: 33–34]

73 Zhang X, Cheng H M, Li J Y, et al. Study on microstructure and mechanical properties of T10 steel quenched by atomized water with nitrogen gas (in Chinese). Hot Work Technol, 2015, 44: 219–222 [张雪, 程赫明, 李建云, 等. T10钢经常压高速气雾淬火工艺处理后组织及性能的研究. 热加工工艺, 2015, 44: 219–222]

74 Zhang L. Research on Fracture Mechanism and Fatigue Performance of Ferritic Ductile Iron (in Chinese). Dissertation for Master's Degree. Chengdu: Southwest Jiaotong University, 2014 [章璐. 铁素体球墨铸铁断裂机理及疲劳性能研究. 硕士学位论文. 成都: 西南交通大学, 2014]

75 Li C L, Qiu F, Chang F, et al. Simultaneously enhanced strength, toughness and ductility of cast 40Cr steels strengthened by trace biphase TiC_x-TiB_2 nanoparticles. Metals, 2018, 8: 707

76 Huang Y L, Sun X F. Study on technology and mechanical performance of hot dipping aluminum coating on 20 steel substrate (in Chinese). J Acad Armored Force Eng, 2016, 30: 117–120 [黄元林, 孙晓峰. 20钢热浸镀铝工艺及力学性能研究. 装甲兵工程学院学报, 2016, 30: 117–120]

77 Li M L. The Evolution Rule and Non-Destructive Detection Method of 20 Steel Strain Aging for Pipes (in Chinese). Dissertation for Doctoral Degree. Jinan: Shandong University, 2012 [李梦丽. 管用20钢应变时效的演化规律及无损检测方法. 博士学位论文. 济南: 山东大学, 2012]

78 Selivorstov V, Dotsenko Y, Borodianskiy K. Influence of low-frequency vibration and modification on solidification and mechanical properties of Al-Si casting alloy. Materials, 2017, 10: 560

79 Soman P P, Herbert E G, Aifantis K E, et al. Analysis of local grain boundary strengthening utilizing the extrinsic indentation size effect. J Mater Res, 2019, 34: 2347–2369

80 Peng Z, Gong J, Miao H. On the description of indentation size effect in hardness testing for ceramics: Analysis of the nanoindentation data. J Eur Ceramic Soc, 2004, 24: 2193–2201

81 Xie Z F. Load Effect on the Translation of Friction Mechanism of GCr15, 304 Stainless, SE NiTi and SME NiTi Alloys (in Chinese). Dissertation for Master's Degree. Chengdu: Southwest Jiaotong University, 2009 [谢祖飞. 载荷对GCr15、 304不锈钢、 SE NiTi和SME NiTi合金摩擦机制转变的影响研究. 硕士学位论文. 成都: 西南交通大学, 2009]

82 Kölemen U. Analysis of ISE in microhardness measurements of bulk MgB_2 superconductors using different models. J Alloys Compd, 2006, 425: 429–435

83 Morales A L, Nieto A J, Chicharro J M, et al. Field-dependent elastic modulus and damping in pure iron, nickel and cobalt. J Magn Magn Mater, 2010, 322: 1952–1961

84 Kong J X, Chen H, He N, et al. Dynamic mechanical property test and constitutive model of pure iron materal (in Chinese). Acta Aeronaut Astronaut Sin, 2014, 35: 2063–2071 [孔金星, 陈辉, 何宁, 等. 纯铁材料动态力学性能测试及本构模型. 航空学报, 2014, 35: 2063–2071]

85 Hadal R S, Misra R D K. Scratch deformation behavior of thermoplastic materials with significant differences in ductility. Mater Sci Eng-A, 2005, 398: 252–261

86 Wong M, Moyse A, Lee F, et al. Study of surface damage of polypropylene under progressive loading. J Mater Sci, 2004, 39: 3293–3308

87 Zhang G, Zhang C, Nardin P, et al. Effects of sliding velocity and applied load on the tribological mechanism of amorphous poly-ether-ether-ketone (PEEK). Tribol Int, 2008, 41: 79–86

88 Nautiyal P, Jain J, Agarwal A. Influence of microstructure on scratch-induced deformation mechanisms in AZ80 magnesium alloy. Tribol Lett, 2016, 61: 29

89 Jiang H, Browning R, Sue H J. Understanding of scratch-induced damage mechanisms in polymers. Polymer, 2009, 50: 4056–4065

90 Tang Y Q, Hu B L, Feng J J. Surface crack analysis in scratch test on Ni-P-Al_2O_3 complex coating surface (in Chinese). J Mech Eng, 2013, 49: 55–62 [谭援强, 胡斌梁, 冯剑军. Ni-P-Al_2O_3复合涂层划痕试验中的表面裂纹分析. 机械工程学报, 2013, 49: 55–62]

91 Lu C P, Gao H, Wang B, et al. Experimental study of single-tip scratching on potassium dihydrogen phosphate single crystal (in Chinese). J Mech Eng, 2010, 46: 179–185 [鲁春朋, 高航, 王奔, 等. 磷酸二氢钾晶体单点划痕试验研究. 机械工程学报, 2010, 46: 179–185]

92 Kobrick R L, Klaus D M, Street K W. Standardization of a volumetric displacement measurement for two-body abrasion scratch test data analysis. Wear, 2011, 270: 650–657

93 Lee K, Marimuthu K P, Kim C L, et al. Scratch-tip-size effect and change of friction coefficient in nano/micro scratch tests using XFEM. Tribol Int, 2018, 120: 398–410

94 Vencl A, Manić N, Popovic V, et al. Possibility of the abrasive wear resistance determination with scratch tester. Tribol Lett, 2009, 37: 591–604

95 Geng Y, Zhang J, Yan Y, et al. Experimental and theoretical investigation of crystallographic orientation dependence of nanoscratching of single crystalline copper. PLoS ONE, 2015, 10: e0131886

96 Nakamura R, Iwabuchi A. Role of graphite in cast iron on tribological behavior in nano-scratch test. JAMDSM, 2012, 6: 1046–1056

97 Ni W, Cheng Y T, Lukitsch M J, et al. Effects of the ratio of hardness to Young's modulus on the friction and wear behavior of bilayer coatings. Appl Phys Lett, 2004, 85: 4028–4030

98 Liu M, Yan F. Comparison of microscratch responses of metals between Berkovich and Rockwell C indenters under progressive normal force. Tribol Lett, 2021, 69: 157

99 Liu M, Yan F W, Gao C H. Effects of progressive normal force on microscratch responses of metallic materials (in Chinese). Acta Metall Sin, 2021, 57: 1333–1342 [刘明, 严富文, 高诚辉. 渐进法向力对金属材料微米划痕响应的影响. 金属学报, 2021, 57: 1333–1342]

100 Khruschov M. Resistance of metals to wear by abrasion, as related to hardness. In: Proceedings of the Conference Lubrication and Wear. Tokyo: Institute of Microelectronics, 1957

101 Li X. Study of the material removal mechanism of glass-ceramics based on consecutive incremental loading in ductile-regime grinding. Nanotechnol Precision Eng, 2020, 3: 88–95

102 Zhu R, Li Y, Zhang X, et al. Strain-rate sensitivity of scratch hardness and deformation mechanism in nanocrystalline Ni under micro-scratch testing. J Mater Sci, 2016, 51: 5889–5900

103 Xu N, Han W, Wang Y, et al. Nanoscratching of copper surface by CeO_2. Acta Mater, 2017, 124: 343–350

104 Mergler Y J, Kampen R J, Nauta W J, et al. Influence of yield strength and toughness on friction and wear of polycarbonate. Wear, 2005, 258: 915–923

105 Liu M, Xie P. Rate and load effects on scratch behavior of thermoplastics by Berkovich indenter. J Materi Eng Perform, 2023, doi: 10.1007/s11665-022-07787-0

106 Liu M, Huang C X, Gao C H. Effect of sample tilt and normal load on micro-scratch test of copper with a spherical indenter (in Chinese). Tribology, 2021, 41: 27–37 [刘明, 黄承馨, 高诚辉. 试样倾斜和正压力对球形压头微米划痕测试紫铜的影响. 摩擦学学报, 2021, 41: 27–37]

107 Flores S E, Pontin M G, Zok F W. Scratching of elastic/plastic materials with hard spherical indenters. J Appl Mech, 2008, 75: 061021

108 Nečas D, Klapetek P. Gwyddion: An open-source software for SPM data analysis. Open Phys, 2012, 10: 181–188

109 Sawamura S, Wondraczek L. Scratch hardness of glass. Phys Rev Mater, 2018, 2: 092601

110 Friedrich K, Sue H J, Liu P, et al. Scratch resistance of high performance polymers. Tribol Int, 2011, 44: 1032–1046

111 Kareer A, Hou X D, Jennett N M, et al. The existence of a lateral size effect and the relationship between indentation and scratch hardness in copper. Philos Mag, 2016, 96: 3396–3413

112 Lindroos M, Valtonen K, Kemppainen A, et al. Wear behavior and work hardening of high strength steels in high stress abrasion. Wear, 2015, 322-323: 32–40

113 Quinn G D, Green P, Xu K. Cracking and the indentation size effect for Knoop hardness of glasses. J Am Ceramic Soc, 2003, 86: 441–448

114 Kim J Y, Kang S K, Lee J J, et al. Influence of surface-roughness on indentation size effect. Acta Mater, 2007, 55: 3555–3562

115 Kurkcu P, Andena L, Pavan A. An experimental investigation of the scratch behaviour of polymers—2: Influence of hard or soft fillers. Wear, 2014, 317: 277–290

116 Kareer A. Nano-scratch hardness and the Lateral Size Effect (LSE). Dissertation for Doctoral Degree. Leicester: University of Leicester, 2015

117 Chen X Q. Influence of chemical composition and annealing process on microstructure and properties of H62 brass (in Chinese). Nonferrous Met Process, 2007, 36: 58–60 [陈秀琴. 化学成分及退火工艺对H62黄铜组织与性能的影响. 有色金属加工, 2007, 36: 58–60]

118 Peng J, Lv B J, Zhu X, et al. Effects of Al content and homogenization on microstructure of the AZ series alloys (in Chinese). J Mater Eng, 2011: 17–22 [彭建, 吕滨江, 朱熹, 等. Al含量及均匀化处理对AZ系列镁合金组织的影响. 材料工程, 2011: 17–22]

119 Zhang G J, Long S Y, Cao F H. Effect of aluminum content on the microsctructure and mechanical properties of AZ magnesium alloys (in Chinese). Spec Cast Nonferrous Alloys, 2009, 29: 848–850 [张广俊, 龙思远, 曹凤红. Al含量对AZ系镁合金组织和力学性能的影响. 特种铸造及有色合金, 2009, 29: 848–850]

120 de Macedo G N B M, Sawamura S, Wondraczek L. Lateral hardness and the scratch resistance of glasses in the Na_2O-CaO-SiO_2 system. J Non-Crystalline Solids, 2018, 492: 94–101

121 Rouxel T, Yokoyama Y. Elastic properties and atomic bonding character in metallic glasses. J Appl Phys, 2015, 118: 044901

122 Parvin M, Williams J G. The effect of temperature on the fracture of polycarbonate. J Mater Sci, 1975, 10: 1883–1888

123 Johnson J A, Jones D W. The mechanical properties of PMMA and its copolymers with ethyl methacrylate and butyl methacrylate. J Mater Sci, 1994, 29: 870–876

124 Xie Q, Sidor J J, Lian J, et al. Self-equilibrated backstresses induce compensation between hardening and softening: Micromechanical and microstructural features. Mater Sci Eng-A, 2022, 843: 143145

125 Dai S J. Effects of high energy shot peening on the microstructure, mechanical properties an wear resistant properties of pure titanium (in Chinese). J Chongqing Univ Technol (Nat Sci), 2018, 32: 116–120, 155 [戴世娟. 高能喷丸处理对纯钛的显微组织、力学和耐磨性能的影响. 重庆理工大学学报(自然科学), 2018, 32: 116–120, 155]

126 Johnson K L, Johnson K L. Contact Mechanics. Cambridge: Cambridge University Press, 1987

127 Bellemare S, Dao M, Suresh S. The frictional sliding response of elasto-plastic materials in contact with a conical indenter. Int J Solids Struct, 2007, 44: 1970–1989

128 Ma Z S, Zhou Y C, Long S G, et al. An inverse approach for extracting elastic-plastic properties of thin films from small scale sharp indentation. J Mater Sci Tech, 2012, 28: 626–635

129 Liu M, Zheng Q, Wang X, et al. Characterization of distribution of residual stress in shot-peened layer of nickel-based single crystal superalloy DD6 by nanoindentation technique. Mech Mater, 2022, 164: 104143

130 Gao X L, Jing X N, Subhash G. Two new expanding cavity models for indentation deformations of elastic strain-hardening materials. Int J Solids Struct, 2006, 43: 2193–2208

131 Liu M, Zheng Q, Gao C H. Charaterization of mechanical properties of bulk metallic glasses based on Knoop hardness (in Chinese). Chin J Solid Mech, 2021, 42: 376–392 [刘明, 郑强, 高诚辉. 基于努氏硬度表征大块金属玻璃的力学性能. 固体力学学报, 2021, 42: 376–392]

132 Fischer-Cripps A C. Nanoindentation. New York: Springer Science+Business Media, 2011

133 Kurkcu P, Andena L, Pavan A. An experimental investigation of the scratch behaviour of polymers: 1. Influence of rate-dependent bulk mechanical properties. Wear, 2012, 290-291: 86–93

Scratch responses of ductile materials by instrumented scratch with a spherical indenter under progressive load

LIU Ming* & XU ZhiTong

Fujian Provincial Key Laboratory of Terahertz Functional Devices and Intelligent Sensing, School of Mechanical Engineering and Automation, Fuzhou University, Fuzhou 350108, China

Under progressive normal load, a spherical indenter (radius of 500 μm) made of zirconia ceramic was used to explore the elastic-plastic deformation of ductile materials including three polymers and twenty metals during instrumented scratch tests. The results of instrumented scratch tests show that as the normal load increases, the elastic recovery ratio, residual scratch hardness, geometric scratch hardness, and lateral scratch hardness of metals can approach constant levels. However, the elastic recovery ratio and geometric scratch hardness of polymers decrease monotonically, possibly due to the occurrence of damage or failure. The fracture toughness values of polymers estimated at the largest normal load based on linear elastic fracture mechanics are consistent with the results in the literature. Under large loads, both residual scratch hardness and lateral scratch hardness of polymers can be approximated as being constant. Residual scratch hardness is found to be larger than geometric scratch hardness. The geometry of a spherical indenter helps explain the nonlinear increase in friction coefficient with increasing applied normal force (the constant levels of friction coefficients for gray and nodular cast irons are mainly caused by the influence of graphite). Most materials' scratch responses are closely related to their mechanical properties: the critical scratch strain (the initial strain of the steady state of elastic recovery ratio) is proportional to yield strain; there is a linear relationship between yield strength and the steady-state residual scratch hardness, which is proportional to Knoop hardness.

instrumented scratch, spherical indenter, progressive load, elastic-plastic deformation, mechanical properties

PACS: 46.35.+z, 46.55.+d, 46.80.+j, 61.41.+e, 62.20.Fe

doi: 10.1360/SSPMA-2022-0402